REPORT DOCUMENTATION PAGE

Form approved
OMB No. 0704-0188

1. AGENCY USE ONLY *(Leave blank)*	2. REPORT DATE	3. REPORT TYPE AND DATES COVERED
		Reprint

4. TITLE AND SUBTITLE

Design of Materials with Extreme Thermal Expansion Using a Three-Phase Topology Optimization Method

5. FUNDING NUMBERS

DAAH04-95-1-0102

6. AUTHOR(S)

Ole Sigmund and Salvatore Torquato

7. PERFORMING ORGANIZATION NAMES(S) AND ADDRESS(ES)

Princeton University
Princeton, NJ 08544

8. PERFORMING ORGANIZATION REPORT NUMBER

9. SPONSORING/MONITORING AGENCY NAME(S) AND ADDRESS(ES)

U.S. Army Research Office
P.O. Box 12211
Research Triangle Park, NC 27709-2211

10. SPONSORING/MONITORING AGENCY REPORT NUMBER

ARo 33905.13-MS-MUR

11. SUPPLEMENTARY NOTES

The views, opinions, and/or findings contained in this report are those of the author(s) and should not be construed as an official Department of the Army position, policy, or decision, unless so designated by other documentation.

12a. DISTRIBUTION/AVAILABILITY STATEMENT

Approved for public release; distribution unlimited.

12b. DISTRIBUTION CODE

13. ABSTRACT *(Maximum 200 words)*

Composites with extremal or unusual thermal expansion coefficients are designed using a three-phase topology optimization method. The composites are made of two different material phases and a void phase. The topology optimization method finds the distribution of material phases optimizing an objective function (e.g., thermoelasticity) subject to certain constraints, such as elastic symmetry or volume fractions of the constituent phases, within a periodic base cell. The effective properties of the material are found using numerical homogenization based on finite-element discretization of the base cell. To benchmark the design method we first consider two-phase designs. Our optimal two-phase microstructures agree well with rigorous bounds and so-called Vigdergauz microstructures that realize the bounds. For three phases, the optimal microstructures are compared with new rigorous bounds and again it is shown that the method yields designed materials with thermoelastic properties close to the bounds. The three-phase design method is illustrated by designing materials having maximum directional thermal expansion (thermal actuators), zero isotropic thermal expansion (thermal actuators), zero isotropic thermal expansion, and negative isotropic thermal expansion. It is shown that materials with effective negative thermal expansion coefficients can be obtained by mixing two phases with positive thermal expansion coefficients and void.

14. SUBJECT TERMS

composites, thermal expansion, topology optimization, actuators, numerical simulation

15. NUMBER OF PAGES

16. PRICE CODE

17. SECURITY CLASSIFICATION OF REPORT	18. SECURITY CLASSIFICATION OF THIS PAGE	19. SECURITY CLASSIFICATION OF ABSTRACT	20. LIMITATION OF ABSTRACT
UNCLASSIFIED	UNCLASSIFIED	UNCLASSIFIED	UNLIMITED

DANISH CENTER FOR APPLIED

MATHEMATICS AND MECHANICS

DESIGN OF MATERIALS WITH EXTREME THERMAL EXPANSION
USING A THREE-PHASE TOPOLOGY OPTIMIZATION METHOD

by

Ole Sigmund and Salvatore Torquato

DCAMM

TECHNICAL UNIVERSITY OF DENMARK

DANISH CENTER FOR
APPLIED MATHEMATICS AND MECHANICS

Scientific Council

Poul Andersen	Dept. of Naval Architecture and Offshore Engineering
Martin P. Bendsøe	Dept. of Mathematics
Esben Byskov	Dept. of Structural Engineering and Materials
Ove Ditlevsen	Dept. of Structural Engineering and Materials
J. Buhr Hansen	Dept. of Hydrodynamics and Water Resources
Ivar G. Jonsson	Dept. of Hydrodynamics and Water Resources
Wolfhard Kliem	Dept. of Mathematics
H. Saustrup Kristensen	Dept. of Energy Engineering
P. Scheel Larsen	Dept. of Energy Engineering
Frithiof I. Niordson	Dept. of Solid Mechanics
Pauli Pedersen	Dept. of Solid Mechanics
P. Terndrup Pedersen	Dept. of Naval Architecture and Offshore Engineering
P. Grove Thomsen	Dept. of Mathematical Modelling
Hans True	Dept. of Mathematical Modelling
Viggo Tvergaard	Dept. of Solid Mechanics

Secretary

Pauli Pedersen, Docent, Dr.techn.
Department of Solid Mechanics, Building 404
Technical University of Denmark
DK−2800 Lyngby, Denmark

DESIGN OF MATERIALS WITH EXTREME THERMAL EXPANSION
USING A THREE-PHASE TOPOLOGY OPTIMIZATION METHOD

by

Ole Sigmund and Salvatore Torquato

SOLID MECHANICS

DTU

TECHNICAL UNIVERSITY OF DENMARK

Design of materials with extreme thermal expansion using a three-phase topology optimization method

O. Sigmund* and S. Torquato
Department of Civil Engineering and Operations Research and
Princeton Materials Institute
Princeton University
Princeton, N.J. 08544, USA

Abstract

Composites with extremal or unusual thermal expansion coefficients are designed using a three-phase topology optimization method. The composites are made of two different material phases and a void phase. The topology optimization method consists in finding the distribution of material phases that optimizes an objective function (e.g., thermoelastic properties) subject to certain constraints, such as elastic symmetry or volume fractions of the constituent phases, within a periodic base cell. The effective properties of the material structures are found using the numerical homogenization method based on a finite-element discretization of the base cell. The optimization problem is solved using sequential linear programming.

To benchmark the design method we first consider two-phase designs. Our optimal two-phase microstructures are in fine agreement with rigorous bounds and the so-called Vigdergauz microstructures that realize the bounds. For three phases, the optimal microstructures are also compared with new rigorous bounds and again it is shown that the method yields designed materials with thermoelastic properties that are close to the bounds.

The three-phase design method is illustrated by designing materials having maximum directional thermal expansion (thermal actuators), zero isotropic thermal expansion, and negative isotropic thermal expansion. It is shown that materials with effective negative thermal expansion coefficients can be obtained by mixing two phases with positive thermal expansion coefficients and void.

---

*Partly on leave from Department of Solid Mechanics, Technical University of Denmark, DK-2800 Lyngby, Denmark (current and permanent address).

1 Introduction

In this paper, we use a topology optimization procedure to determine the distribution of three phases (two different bulk material phases and a void phase) in order to design composites with extremal or unusual thermal expansion behavior. Three phases are used (as opposed to two phases) since one can achieve effective properties of the composite beyond those of the individual components [25]. Microstructural variation is limited to one length scale in a unit cell as this is most easily manufacturable.

Materials with extreme or unusual thermal expansion behavior are of interest from both a technological and fundamental standpoint. Of particular practical interest are materials with zero thermal expansion, maximum thermal expansion or force, and negative (i.e., minimum) thermal expansion. Heretofore, however, a systematic procedure to design materials with exotic thermal-expansion behavior has been lacking.

Materials with *zero thermal expansion coefficients* are needed for use in structures subject to temperature changes such as civil engineering and space structures as well as piping systems. Examples are bridges, where temperature changes between day and night, and summer and winter, cause big structural changes, and space applications, where temperature differences between sunny and shady sides of a structure are extreme. Such temperature differences can cause distortion of space antennas and "rapid" temperature changes due to orbit of the Hubble space telescope are known to cause thermal distortions of its solar arrays in turn causing the arrays and thereby the telescope to vibrate (Collins and Richter [8]). Materials with *maximum unidirectional thermal displacement or force* can be employed as "thermal" actuators. Materials with negative thermal expansion coefficients can be used to overcome positive thermal expansion of other materials or, among other applications, be used for thermally operated fasteners. A fastener made of a negative thermal expansion coefficient material, upon heating, can be inserted easily into a hole because of the volume contraction. When cooled down, it will expand, fitting tightly into the hole and upon heating can be easily removed. Finally, the design of material with specific thermal expansion coefficients is important, to be able to eliminate thermal mismatch between parts in structures subject to heat changes.

A negative thermal expansion material has the counterintuitive property of contracting upon heating. There are a number of existing materials with negative thermal expansion coefficients. Glasses in the titania-silica family have isotropic negative expansion coefficients at *room temperature* [40]. Examples of materials that have negative thermal expansion at very low temperatures ($< 100K$) are silicon and germanium [22] as well as $Bi_{2.2}Sr_{1.8}CaCu_2O_x$ superconductor single crystals [48]. Examples of materials with *directional* negative thermal expansion coefficients at room temperature are Kevlar, carbon fibers, plastically deformed (anisotropic) Invar (Fe-Ni alloys) [18] and certain molecular crystalline networks [3]. The negative expansion mechanism of these molecular-level networks is based on un-twisting of helical chains. Currently there is no way to manufacture these materials in extended form, but this an active area of research.

An interesting question [3] is whether there is a mechanistic relationship between negative thermal expansion and negative Poisson's ratio? A material with negative Poisson's ratio expands laterally when pulled axially and can be manufactured by processing of open-walled foam structures described by Lakes [24]. We will show that isotropic materials with effective

negative thermal expansion coefficients exist with positive values of the Poisson's ratio and that they can be obtained by mixing two phases with positive thermal expansion coefficients and void.

Several researchers have addressed the problem of designing materials composites with specific *directional* thermal expansion properties. Autio, Laitinen and Pramila [2] designed laminates with specific elastic and thermal expansion coefficients by varying layering thicknesses and directions. Wetherhold and Wang [47] tailored the thermal deformation of beams, and Parton and Kudryavtsev [31] discussed the design of one dimensional beams with negative thermal expansion. Rodriques and Fernandes [34] designed thermally loaded structures with optimal stiffness.

It was shown by Levin [27] and later by Rosen and Hashin [35], that there is a simple relationship between the effective thermal expansion coefficients and the effective elastic moduli of *two-phase* materials. In other words, designing two-phase composites with extreme thermal expansion coefficients corresponds to designing two-phase composites with extreme bulk moduli. The problem of finding the structures that extremize the effective elastic properties of two-phase media has a long history beginning with the composite-sphere assemblages of Hashin and Shtrikman [17] for the bulk modulus problem. Certain hierarchical laminates were shown to realize the Hashin-Shtrikman bounds on both the bulk and shear moduli of isotropic two-phase composites [10]. More recently, Milton and Cherkaev [28] have found multi-length scale materials possessing elastic properties ranging over the entire range compatible with thermodynamics. Vigdergauz [45, 46] and Grabovsky and Kohn [12, 13] have studied single-inclusion microstructures of extreme rigidity. Sigmund [41, 42, 43] has designed material structures with specific elastic properties (including isotropic negative Poisson's ratio material), where the microstructure is restricted to one length scale.

For three-phase materials, one-to-one relationships between the thermal expansion coefficients and elastic properties do not exist. Indeed, for multiphase composites, Schapery [38] and Rosen and Hashin [35] found bounds on the thermal expansion coefficients in terms of the stiffness tensor. Recently, Gibiansky and Torquato [11] have improved upon the Rosen-Hashin bounds using the so-called translation method. This improvement was actually motivated by the topology optimization results of the present study. To our knowledge, no one to date has addressed the problem of systematically designing three-phase materials with extreme *isotropic* thermal expansion coefficients.

In this paper, we show how composites with extremal or unusual thermal expansion coefficients can be designed using a three-phase topology optimization method based on the aforementioned works of Sigmund. The three phases consist of two different material phases and void. The two material phases can have different elastic and thermal expansion coefficients, described by their elastic tensors $C_{ijkl}^{(1)}$ and $C_{ijkl}^{(2)}$ and their thermal strain coefficient tensors $\alpha_{ij}^{(1)}$ and $\alpha_{ij}^{(2)}$, respectively. The basic goal is to maximize or minimize components, or combination of components, of the effective thermal strain tensor $\alpha_{ij}^{(*)}$ or effective stress tensor $\beta_{ij}^{(*)} = C_{ijkl}^{(*)} \alpha_{kl}^{(*)}$, subject to constraints on phase volume fractions, effective stiffness and elastic symmetry. To check the validity of the optimization procedure, our results will be compared with the available bounds on thermoelastic properties for three-phase materials [11, 35, 38].

3

The topology optimization procedure proposed here, essentially follows the steps of conventional topology optimization procedures. The design problem is initialized by defining a design domain discretized by a number of finite elements. The optimization procedure then consists in solving a sequence of finite-element problems followed by changes in density and material type of each of the finite elements, dependent on the local strain energies. For simple compliance optimization, this corresponds to adding material where the strain energy density is high and removing material where the strain energy density is low.

The proposed procedure differs from the conventional approach in an important aspect. In the original works on topology optimization (e.g. Bendsøe and Kikuchi [4] and Kohn and Strang [23]), elimination of ill-conditioning and the existence of materials in elements of intermediate densities was ensured by using so-called ranked materials made of microscopically oscillating material on differing length scales or by using microstructures with rectangular holes. Using homogenization methods to determine the effective properties of ranked (or microstructured) materials and substituting the homogenized parameters into the "macroscopic" topology optimization problem, lead to the "homogenization approach to topology optimization". In this paper, however, we will use an "artificial" material model for intermediate densities which means that the material properties in a given element is simply some fraction times the material properties of solid material. As long as we end up having entirely solid material or void in each element, this is a perfectly valid approach. By using the "artificial-material" model, we simplify the whole design procedure significantly because the local problems of determining lamination parameters and orientations at different length scales of the ranked materials are eliminated. The "artificial-material" model has been used by several authors (e.g. Rozvany et al. [36], Mlejnek and Schirrmacher [29] and Sigmund [41]).

At each step of the topology optimization procedure, we have to determine the effective thermoelastic properties of the microstructure. There exist several methods to determine these properties. However, because the topology optimization method is based on finite-element discretizations, and because the finite-element method allows easy derivation and evaluation of the sensitivities of the effective properties with respect to design changes, we have chosen to use a finite element based numerical homogenization procedure as developed in Bourgat [6] and Guedes and Kikuchi [14].

The paper is organized the following way. In section 2 we describe the three-phase topology optimization procedure and its application to design of material structures with extreme thermal expansion. The sequential linear programming method used to solve the topology optimization problem is described in section 2.2 and numerical implementation issues are discussed in section 2.3. Solving the topology optimization procedure as proposed, results in solutions with finite-element related problems such as checkerboards, mesh-dependency and local optima. These problems and procedures to avoid them are discussed in section 2.4. To benchmark the optimization procedure, results obtained are compared to bounds for two and three phase materials; the available bounds are listed in section 3. The performance of the design procedure is demonstrated by several examples in section 4. The calculation of the effective thermoelastic properties using a numerical homogenization procedure based on the finite-element method is briefly described in Appendix A and the sensitivity analysis necessary to solve the design problem is listed in Appendix B.

4

2 Procedures for three-phase topology optimization

This section describes a numerical procedure for topology optimization of three-phase material structures in two dimensions. A sequential linear programming problem is formulated to solve the optimization problem. The procedure is applied to the design of material structures with extreme thermal expansion properties. For the derivations, we will assume that we can find the effective stiffness and thermal expansion tensors $C_{ijkl}^{(*)}$, $\alpha_{ij}^{(*)}$ and $\beta_{ij}^{(*)}$ using the numerical homogenization method described in Appendix A. The sensitivity analysis necessary for solving the problem is derived in Appendix B. At the end of the section, we discuss implementation issues as well as some numerical difficulties and how to avoid them.

Assuming two-dimensional linear elasticity (i.e. small strains), perfect bonding between the material phases, uniform temperature distribution and constant material properties, the thermoelastic behavior of materials can be described by the constitutive relations given as

$$\sigma_{ij} = C_{ijkl}\epsilon_{kl} - C_{ijkl}\alpha_{kl}\Delta T = C_{ijkl}\epsilon_{kl} - \beta_{ij}\Delta T, \tag{1}$$

where C_{ijkl}, σ_{ij}, ϵ_{kl}, α_{kl}, β_{ij} are the elasticity, stress, strain, thermal strain, and thermal stress tensors, respectively, and ΔT is the temperature change. We refer to α_{kl} as the "thermal strain tensor" (the resulting strain of a material which is allowed to expand freely) and to β_{ij} as the "thermal stress tensor" (the stress in a material which is not allowed to expand). For the three-phase composite of interest, the constitutive equation Eq. (1) is valid on a local scale (with superscripts (0), (1), and (2) appended to the thermoelastic properties, i.e. $C_{ijkl}^{(m)}$, $\alpha_{ij}^{(m)}$ and $\beta_{ij}^{(m)}$) and the macroscopic scale (with superscript (*) appended to the properties). In the latter case, the stresses and strains are averages over local stresses and strains, respectively, i.e.

$$\overline{\sigma}_{ij} = C_{ijkl}^{(*)}\overline{\epsilon}_{kl} - C_{ijkl}^{(*)}\alpha_{kl}^{(*)}\Delta T = C_{ijkl}^{(*)}\overline{\epsilon}_{kl} - \beta_{ij}^{(*)}\Delta T, \tag{2}$$

where overbar denotes the volume average. The effective thermoelastic properties, $C_{ijkl}^{(*)}$, $\alpha_{kl}^{(*)}$ and $\beta_{ij}^{(*)}$ of the three phase composite are computed using a numerical homogenization method as described in Appendix A.

The goal of this work is to optimize components or combinations of components of the effective thermal tensors $\alpha_{ij}^{(*)}$ or $\beta_{ij}^{(*)}$ by distributing, in a clever way, given amounts of two material phases and void within the design domain representing a base cell of a periodic material. In other words, we want to design microstructural topologies that give us some desirable overall thermoelastic properties. As will be seen later, materials with extreme thermal expansion tend to have low overall stiffness. Thus, for practical applications, one must bound the effective stiffness or bulk moduli from below. It should also be possible to specify elastic symmetries such as orthotropy, square symmetry or isotropy of the resulting materials.

An optimization problem including these features can be written as

$Minimize$: Some function of $\alpha_{ij}^{(*)}$ or $\beta_{ij}^{(*)}$,

$Variables$: Distribution of two material phases and void in the base cell,

$Subject\ to$: Constraints on volume fractions,

         : Orthotropy, square symmetry or isotropy constraints,   (3)

         : Lower bound constraints on stiffness,

         : Bounds on design variables.

2.1 Formulation of the optimization problem

This subsection discusses the individual parts of the optimization problem defined in Eq. (3).

Objective function

The objective function $f(\alpha_{ij}^{(*)}, \beta_{ij}^{(*)})$ can be any combination of the thermal coefficients $\alpha_{ij}^{(*)}$ or $\beta_{ij}^{(*)}$. An example will be the case where we want to minimize the isotropic thermal expansion, i.e. the sum of the thermal strain coefficients in the horizontal and the vertical directions. In that case, the objective function will be $f(\alpha_{ij}^{(*)}) = \alpha_{11}^{(*)} + \alpha_{22}^{(*)}$, where subscripts 11 and 22 define horizontal and vertical directions, respectively. As another example we might consider the maximization of the thermal stress coefficient in the vertical direction. In this case, the objective function will be $f(\beta_{ij}^{(*)}) = -\beta_{22}^{(*)}$ where the minus sign is used to convert the maximization problem into a minimization problem.

Design variables and mixture assumption

Phase 1 material has the stiffness tensor $C_{ijkl}^{(1)}$ and the thermal strain coefficient tensor $\alpha_{ij}^{(1)}$ and similarly phase 2 material has the material tensors $C_{ijkl}^{(2)}$ and $\alpha_{ij}^{(2)}$. The stiffness tensor of the "void" phase is taken as a small number x_{min} times $C_{ijkl}^{(1)}$, respectively, where $x_{min} = 10^{-4}$, for reasons which will be explained later.

The material type, that is, material phase 1, phase 2 or void, can vary from finite element to finite element as seen in Fig. 1. With a fine finite-element discretization, this allows us to define complicated bimaterial topologies within the design domain. Having discretized the design domain (the periodic base cell) with N finite elements, the design problem consists in assigning either phase 1, 2 or void to each element such that the objective function is minimized.

Even for a small number of elements, this integer-type optimization problems becomes a huge combinatorial problem which is impossible to solve. For a small design problem with $N = 100$, the number of different distributions of the three material phases would be astronomical ($3^{100} = 5 \cdot 10^{47}$). As each function evaluation requires a full finite element analysis, it is hopeless to solve the optimization problem using random search methods such as, genetic algorithms or simulated annealing methods, which use a large number of function evaluations and do not make use of sensitivity information. Following the idea of standard topology optimization procedures, the problem is therefore relaxed by allowing the
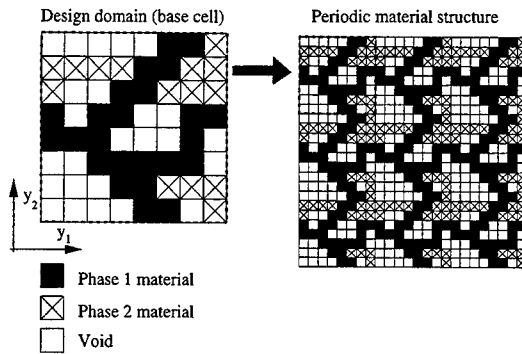
6

Figure 1: Design domain and discretization for the three-phase topology optimization problem. Each square represents one finite element which can consist of either phase 1 or 2 material or void.

material at a given point to be a mixture of the three phases. This makes it possible to find sensitivities with respect to design changes, which in turn allows us to use mathematical programming methods to solve the optimization problem. At the end of the optimization procedure however, we hope to have a design where each element is either void, phase 1 or phase 2 material.

Using a simple artificial mixture assumption, the local stiffness and thermal strain coefficient tensors in element e can be written as a function of the two design variables x_1^e and x_2^e

$$
\begin{aligned}
C_{ijkl}^e(x_1^e, x_2^e) &= (x_1^e)^\eta \left[(1 - x_2^e)C_{ijkl}^{(1)} + x_2^e C_{ijkl}^{(2)}\right], \\
\\
\alpha_{ij}^e(x_2^e) &= (1 - x_2^e)\alpha_{ij}^{(1)} + x_2^e \alpha_{ij}^{(2)},
\end{aligned}
\tag{4}
$$

where η is a penalization factor discussed later. The variable $x_1^e \in [x_{min}, 1]$ can be seen as a local density variable with $x_1^e = x_{min}$ meaning that the given element is "void" and $x_1^e = 1$ meaning that the given element is solid material. The variable $x_2^e \in [0, 1]$ is a "mixture coefficient" with $x_2^e = 0$ meaning that the given element is pure phase 1 material and $x_2^e = 1$ meaning that it is pure phase 2 material. The local thermal strain tensor $\alpha_{ij}^e(x_2^e)$ is not dependent on the density variable x_1^e. This can be explained by the fact that once we have chosen the local material mixture (i.e. the value of x_2^e), the thermal strain coefficient does not change with density.

It should be emphasized that the local material assumptions Eqs. (4) only are valid for the design variables taking the extreme values.[1] Nevertheless, during the design process we allow intermediate values meaning that we are working with artificial (non-existing)

---

[1] A material with constitutive behavior close to the described could be realized as an isotropic porous triangular microstructure

7

materials. This violation is not critical as long as we end up with a discrete design as discussed in the introduction.

Experience shows that the penalty parameter η should be given values ranging from 3 to 10 depending on the design problem. The influence of the penalty parameter can be explained as follows: Let us assume that $x_2^e = 0$ in element e. The local stiffness tensors dependence of x_1^e [Eq. (4)] can then be written as $C_{ijkl}^e(x_1^e) = (x_1^e)^\eta C_{(ijkl)}^{(1)}$. By specifying a value of η higher than one, the local stiffness for fixed $x_1^e < 1$ is lowered, thus making it "uneconomical" to have intermediate densities in the optimal design.

Constraints on volume fractions

Having defined the design variables x_1 and x_2 above, and assuming that the design domain has been disrectized by N finite elements of volume Y^e, the volume fractions of the three phases can be calculated as the sums

$$c^{(1)} = \frac{1}{Y} \sum_{e=1}^{N} x_1^e (1 - x_2^e) Y^e, \qquad c^{(2)} = \frac{1}{Y} \sum_{e=1}^{N} x_1^e x_2^e Y^e, \qquad c^{(0)} = 1 - c^{(1)} - c^{(2)}, \qquad (5)$$

where Y is the volume of the base cell. For a specific design problem, we might want to constrain the volume fractions of the phases. This can be done by defining two volume fraction constraints as

$$c_{min}^{(1)} \le c^{(1)} \le c_{max}^{(1)}, \qquad c_{min}^{(2)} \le c^{(2)} \le c_{max}^{(2)}, \qquad (6)$$

where $c_{min}^{(1)}$, $c_{min}^{(2)}$, $c_{max}^{(1)}$ and $c_{max}^{(2)}$ are lower and upper bounds on the volume fractions of material 1 and 2, respectively. By setting the lower bound constraint equal to the upper bound constraint, it is possible to fix the volume fractions of the individual phases.

Isotropy or square symmetry constraints

For the purpose of designing materials with either orthotropic, square symmetric or isotropic elastic parameters, such constraints must be implemented in the optimization problem. Orthotropy of the materials can be obtained simply by specifying at least one geometrical symmetry axis in the base cell. Assuming that a material structure is orthotropic, the condition for square symmetry of the elasticity tensor is that $C_{1111}^{(*)} - C_{2222}^{(*)} = 0$, and the conditions for isotropy of the elasticity tensor under plane stress assumption are that $C_{1111}^{(*)} - C_{2222}^{(*)} = 0$ and $(C_{1111}^{(*)} + C_{2222}^{(*)}) - 2(C_{1122}^{(*)} + 2C_{1212}^{(*)}) = 0$. Finally, the condition for thermal expansion isotropy is that $\alpha_{11}^{(*)} - \alpha_{22}^{(*)} = 0$ and $\alpha_{12}^{(*)} = 0$. These conditions are difficult to implement as equality constraints in an optimization problem because the starting guess might be infeasible (i.e. anisotropic). Therefore, it is chosen to implement the constraints as a penalty function added to the cost function. The penalty function is defined as the squared error in obtaining either square symmetry, elastic or thermal isotropy, times the penalization factors r_1, r_2 and r_3, respectively. It should be noted here that three 60 degree symmetry lines of a microstructure is a sufficient but not a necessary condition for isotropy. Indeed, this paper shows examples of isotropic material structures with only one line of symmetry.

The errors in obtaining square symmetry or isotropy, respectively, can be written as

$$Error_{sq} \;=\; \frac{(C_{1111}^{(*)} - C_{2222}^{(*)})^2}{(C_{1111}^{(*)} + C_{2222}^{(*)})^2}, \tag{7}$$

$$Error_{iso} \;=\; \frac{\left[(C_{1111}^{(*)} + C_{2222}^{(*)}) - 2(C_{1122}^{(*)} + 2C_{1212}^{(*)})\right]^2}{(C_{1111}^{(*)} + C_{2222}^{(*)})^2} + Error_{sq}.$$

Expressions similar to $Error_{sq}$ and $Error_{iso}$ are also known in the literature of composite materials (e.g. Christensen [7]) as the practical composite parameters U_2 and U_3.

The error in obtaining isotropic thermal expansion can be defined as

$$Error_{therm} = \frac{(\alpha_{12}^{(*)})^2 + (\alpha_{11}^{(*)} - \alpha_{22}^{(*)})^2}{(\alpha_{11}^{(*)} + \alpha_{22}^{(*)})^2} \tag{8}$$

Lower bound constraints on effective stiffness

As will be seen later, extreme thermal properties can be obtained if we allow the overall stiffness of the material to be small. Low stiffness is generally undesirable and therefore we will introduce a lower bound constraint on the the directional Young's moduli $E_1^{(*)}$ and $E_2^{(*)}$ or on the bulk modulus $k^{(*)}$ of the material.

Such constraints can be written as $g_{i(min)} \leq g_i(C_{ijkl}^{(*)})$. For isotropic materials, we have a lower bound constraint on the bulk modulus $[k_{min}^{(*)} \leq k^{(*)} = (C_{1111}^{(*)} + C_{2222}^{(*)})/2 + C_{1122}^{(*)}]$. For anisotropic materials, we might want to constrain the value of the horizontal or vertical Young's moduli, i.e. $[E_{min(1)}^{(*)} \leq E_1^{(*)} = C_{1111}^{(*)} - (C_{1122}^{(*)})^2/C_{2222}^{(*)}]$ or $[E_{min(2)}^{(*)} \leq E_2^{(*)} = C_{2222}^{(*)} - (C_{1122}^{(*)})^2/C_{1111}^{(*)}]$.

Lower bound constraints on design variables

For computational reasons (singularity of the stiffness matrix in the finite element formulation), the lower bound on design variable x_1^e is set to x_{min}; not zero ($x_{min} = 10^{-4}$). Numerical experiments show that the "void" regions have practically no structural significance and can be regarded as real void regions. The bounds on the design variables can thus be written as $0 < x_{min} \leq x_1^e \leq 1$ and $0 \leq x_2^e \leq 1$.

The final optimization problem

An optimization problem including above mentioned features can now be written as

$$
\begin{aligned}
Minimize \quad &: \quad \Phi(\mathbf{x}_1, \mathbf{x}_2) = f(\alpha_{ij}^{(*)}, \; \beta_{ij}^{(*)}) + r_1 Error_{sqr} + r_2 Error_{iso} + r_3 Error_{therm}, \\
subject \; to \quad &: \quad g_{i(min)} \leq g_i(C_{ijkl}^{(*)}), \; i = 1, \ldots, M, \\
&: \quad c_{min}^{(1)} \leq c^{(1)} \leq c_{max}^{(1)}, \\
&: \quad c_{min}^{(2)} \leq c^{(2)} \leq c_{max}^{(2)}, \\
&: \quad \mathbf{0 < x}_{min} \leq \mathbf{x}_1 \leq \mathbf{1}, \\
&: \quad \mathbf{0 \leq x}_2 \leq \mathbf{1},
\end{aligned}
\tag{9}
$$

where $\mathbf{x}_1$ and $\mathbf{x}_2$ are the N-vectors containing the design variables and the three penalty parameters r_i can be set to zero or non-zero values, depending on the desired isotropy type.

2.2 Sequential linear programming method

Topology optimization problems in the literature often consist in the optimization of a simple energy functional (e.g. compliance or eigenfrequencies) with a single constraint on material resource, and these problems can therefore be solved very efficiently using optimality criteria methods. In this paper, however, we are considering several different objective functions and multiple constraints which can not be written in energy forms and therefore it will be cumbersome if not impossible to formulate the optimization problem as an optimality criteria problem. Instead we will use a mathematical programming method called sequential linear programming (SLP), which consists in the sequential solving of an approximate linear sub-problem, obtained by writing linear Taylor series expansions for the objective and constraint functions. The SLP method was successfully used in optimization of truss structures by Pedersen [32] and was evaluated as a robust, efficient and easy to use optimization algorithm in a review paper by Schittkowski [39].

Using the sequential linear programming method, the optimization problem Eq. (9) is solved iteratively. In each iteration step, the optimization problem is linearized around the current design point $\{\mathbf{x}_1, \mathbf{x}_2\}$ using the first part of a Taylor series expansion and the vector of optimal design changes $\{\Delta\mathbf{x}_1, \Delta\mathbf{x}_2\}$ is found by solving the linear programming problem

$$
\begin{aligned}
Minimize \quad &: \quad \Phi + \left\{ \frac{\partial\Phi}{\partial\mathbf{x}_1}, \frac{\partial\Phi}{\partial\mathbf{x}_2} \right\}^T \{\Delta\mathbf{x}_1, \Delta\mathbf{x}_2\}, \\
subject\ to \quad &: \quad g_{i(min)} - g_i \leq \left\{ \frac{\partial g}{\partial\mathbf{x}_1}, \frac{\partial g}{\partial\mathbf{x}_2} \right\}^T \{\Delta\mathbf{x}_1, \Delta\mathbf{x}_2\},\ i = 1, \ldots, M, \\
&: \quad c_{min}^{(1)} - c^{(1)} \leq \left\{ \frac{\partial c^{(1)}}{\partial\mathbf{x}_1}, \frac{\partial c^{(1)}}{\partial\mathbf{x}_2} \right\}^T \{\Delta\mathbf{x}_1, \Delta\mathbf{x}_2\} \leq c_{max}^{(1)} - c^{(1)}, \quad (10) \\
&: \quad c_{2min} - c^{(2)} \leq \left\{ \frac{\partial c^{(2)}}{\partial\mathbf{x}_1}, \frac{\partial c^{(2)}}{\partial\mathbf{x}_2} \right\}^T \{\Delta\mathbf{x}_1, \Delta\mathbf{x}_2\} \leq c_{2max} - c^{(2)}, \\
&: \quad \{\Delta\mathbf{x}_{1L}, \Delta\mathbf{x}_{2L}\} \leq \{\Delta\mathbf{x}_1, \Delta\mathbf{x}_2\} \leq \{\Delta\mathbf{x}_{1U}, \Delta\mathbf{x}_{2U}\},
\end{aligned}
$$

where $\Delta\mathbf{x}_{1L}$, $\Delta\mathbf{x}_{2L}$, $\Delta\mathbf{x}_{1U}$ and $\Delta\mathbf{x}_{2U}$ are move-limits on the design variables. The move-limits are adjusted for the absolute limits given in Eqs. (9).

The applied move-limit strategy is important for the stable convergence of the algorithm. Here we use the simple rule that the move-limit for a specific design variable is increased by a factor of 1.4 if the change in the design variable has the same sign for two subsequent steps. Similarly the move-limit is decreased by a factor of 0.6 if the change in the design variable has opposite signs for two subsequent steps.

The sensitivities, which are necessary to solve the linearized sub-problem Eq. (10), are derived in Appendix B, and are calculated locally for each element. This means that no additional finite-element problems have to be solved to find the sensitivities needed.
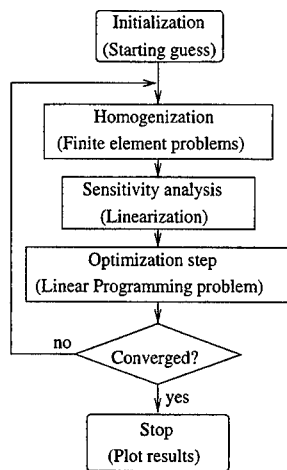
Figure 2: Flowchart of the design algorithm

2.3 Numerical implementation issues

This subsection describes the numerical implementation of the three-phase topology optimization problem including the finite-element discretization and procedures, the linear programming package DSPLP [16] from the SLATEC library, control of move-limits and a flowchart of the procedure.

A flowchart of the design algorithm is shown in Fig. 2. The individual steps of the design procedure are described in the following.

Initialization

First, we initialize the design problem by selecting the objective function, specifying a lower bound on the stiffness, selecting isotropy type and symmetry lines. We also choose the design domain discretization, using 900 or 3600 4-node linear displacement finite elements, corresponding to 30 by 30 or 60 by 60 element discretizations, depending on accuracy demands and available computing time. To save computer time, a design problem can first be solved on a 30 by 30 element mesh. When a solution has been reached, each of the elements are divided into four and the procedure is continued until convergence.

Starting guess

Starting distribution of densities and material types (i.e. starting values of the design variable vectors x_1 and x_2) is up to the user. Having absolutely no idea of what the solution will look like, a random distribution of densities and material types is chosen as the starting guess. If

11

the user has an idea of what the solution will look like or he has an old solution to a similar problem, considerable amount of computing time is saved by using this (old) topology as a starting guess.

Homogenization step

The equilibrium equations Eqs. (17) for the homogenization problem derived in Appendix A, are solved using the finite-element method applied to calculation of effective material properties in Bourgat [6] and Guedes and Kikuchi [14].

Sensitivity analysis

The sensitivity analysis necessary to solve the linear programming problem in Eq. (10) is derived in Appendix B. The computation of the sensitivities is fast because they can be found from the strain fields already computed by the homogenization procedure.

Linear programming problem

The linear programming problem Eq. (10) is solved using a linear programming solver DSPLP [16] from the SLATEC library. As the optimization is non-sparse, the DSPLP routine is invoked with an option for no sparsity. Nevertheless, the routine has proven faster and demands less storage space than other LP-algorithms tests.

Convergence

The iterative design procedure is repeated until the change in each design variable from step to step is lower than 10^{-4} (by experience).

2.4 Problems related to topology optimization

This subsection discusses some numerical difficulties due to the finite-element discretization, namely checkerboard patterns, mesh-dependencies and local minima.

The checkerboard and mesh-dependency problems

Applying the topology optimization method to different design problems, one often encounters regions of alternating solid and void elements, referred to as checkerboards, in the "optimal solutions". The regions are seen in many works on general topology optimization and it was earlier believed, that such regions represented optimal microstructure on the finite-element level. However, two recent papers by Jog and Haber [21] and Díaz and Sigmund [9] conclude, that regions with checkerboard patterns have artificially high (numerical) stiffness (higher than the theoretical bounds) and can be explained by poor numerical modelling of the stiffness of checkerboards by lower order finite elements. Both papers conclude, that checkerboards are certainly prone to appear in topology optimization using four-node finite elements, as here, but also using higher order elements such as nine-node quadratic displacement finite elements.

Another problem, due to the finite-element discretization, is mesh-dependency, which refers to the non-convergence of solutions with mesh-refinement. Refining the finite-element mesh should ideally result in the same topology as for a coarse mesh but with better definitions of the boundaries between the material phases. However, a refinement does result in a solution with a more complicated (finer) microstructure. Methods to avoid this problem have been suggested in three recent papers. Jog, Haber and Bendsøe [15] suggest to introduce a constraint on global perimeter. In a paper on bone remodelling, closely related to topology optimization methods, Mullender, Huiskes and Weihnans [30] suggest a mesh-independency algorithm that assumes that bone growth at a point is dependent on the loads in a (mesh-independent) neighborhood of the point. A method related to the latter approach, but with different origin, is proposed in Sigmund [41], who performs the density update based on low-pass filtered strain energy fields. To avoid the checkerboard and mesh-dependency problems, we use the method suggested in Sigmund [41]

Local minima

The topology optimization problem is very prone to converge to local minima. However, introducing the mesh-independency algorithm (Sigmund [41]) makes it possible to prevent this problem to a certain extent. Solving a cell design problem is typically done as follows. First we solve the optimization problem with a low value of the low-pass filter parameter, i.e., we do not allow rapid variation in the element densities. This results in a design with large areas of intermediate densities but it also prevents the design in converging to a local minimum (binary design). Gradually, we increase the low-pass filter parameter, in turn letting the design problem converge. In that way, we gradually arrive at a solution which is entirely binary and which is, hopefully, a global optimum. To make sure that the actually obtained microstructures are global optima indeed, the same optimization problem is always solved using differing starting guesses, move-limit strategies and choices of low-pass filter parameter and penalty parameter η. However, as will be seen later, topologically different solutions with similar values of the objective function have been found when solving specific design problems. Solutions which are "shifted" (translated half a base cell dimension) of other solutions have also been encountered. The fact that the effective properties of the design examples are close to theoretical bounds supports our belief, that we are finding the optimal topologies with the proposed design procedure.

Computing time

One design iteration, typically takes three seconds (30 by 30 element discretization) and 20 seconds (60 by 60 element discretization) on an Indigo 2 work station. To arrive at an optimal solution, depending on starting guess, several thousand iterations are needed. Including interaction by the user, a full design process may take two working days. Comparing the computing time and number of iterations with other works in topology optimization it can be concluded that the present procedure is extremely slow. However, these other works in topology optimization usually consider self-adjoint loading problems and statically determinant structures where a solution can be found often within a few design iterations. This is due to the fact that the stress fields of statically determinate structures do not change much

13

with design. In this paper, however, the optimal strain and stress fields for the given design problem are unknown in the beginning and must emerge gradually during the design process together with the optimal material distribution.

3 Rigorous expressions and bounds on effective thermoelastic properties

Rigorous expressions for the effective thermal expansion coefficients of two-phase, *isotropic* composites and rigorous bounds on the effective coefficients of three-phase, *isotropic* composites will serve to benchmark the design algorithm. For simplicity, we assume that the constituent phases are isotropic which implies that they can be described by their Young's moduli $E^{(0)}$, $E^{(1)}$ and $E^{(2)}$, their Poisson's ratios $\nu^{(0)}$, $\nu^{(1)}$ and $\nu^{(2)}$ and their thermal strain coefficients $\alpha^{(0)}$, $\alpha^{(1)}$ and $\alpha^{(2)}$. It is also assumed that the composite is macropicically isotropic. The bulk and shear moduli of the phases are then

$$k^{(i)} = \frac{E^{(i)}}{2(1 - \nu^{(i)})}, \qquad \mu^{(i)} = \frac{E^{(i)}}{2(1 + \nu^{(i)})}, \qquad i = 0, 1, 2. \tag{11}$$

Two-phase materials

The effective thermal strain coefficient $\alpha^{(*)}$ of a two-phase isotropic material is explicitly given in terms of the effective bulk modulus $k^{(*)}$ (Levin [27] or Rosen and Hashin [35])

$$\alpha^{(*)} = \frac{\alpha^{(1)} k^{(1)} \left(k^{(2)} - k^{(*)} \right) - \alpha^{(2)} k^{(2)} \left(k^{(1)} - k^{(*)} \right)}{k^{(*)} \left(k^{(2)} - k^{(1)} \right)}. \tag{12}$$

The best bounds on the isotropic effective bulk modulus $k^{(*)}$, given volume fraction information only, were derived by Hashin and Shtrikman [17] and read

$$\left(\overline{\left(\frac{1}{k + \mu_{min}} \right)} \right)^{-1} - \mu_{min} \leq k^{(*)} \leq \left(\overline{\left(\frac{1}{k + \mu_{max}} \right)} \right)^{-1} - \mu_{max}, \tag{13}$$

where bars denote averaged values and μ_{min} and μ_{max} are the minimum and maximum shear moduli [Eq. (11)] of the three phases, respectively. Bounds for the thermal strain coefficient are therefore obtained by inserting the upper and lower bounds for the bulk modulus Eq. (13) into Eq. (12).

Three-phase materials

Bounds on the effective thermal strain coefficient $\alpha^{(L)} \leq \alpha^{(*)} \leq \alpha^{(U)}$ of three-phase, isotropic composites were found by Schapery [38] and Rosen and Hashin [35] and read

$$\left. \begin{array}{c} \alpha^{(U)} \\ \alpha^{(L)} \end{array} \right\} = \frac{1}{(\overline{1/k}) - 1/\overline{k}} \left\{ \overline{\alpha} \left(\frac{1}{k^{(*)}} - \frac{1}{\overline{k}} \right) + \frac{\overline{k\alpha}}{\overline{k}} \left(\overline{\left(\frac{1}{k} \right)} - \frac{1}{k^{(*)}} \right) \pm \right.$$
$$\left. \Psi \left(\overline{\left(\frac{1}{k} \right)} - \frac{1}{k^{(*)}} \right)^{1/2} \left(\frac{1}{k^{(*)}} - \frac{1}{\overline{k}} \right)^{1/2} \right\}, \tag{14}$$

14

where

$$\Psi = \left\{ \left(\overline{\left(\frac{1}{k}\right)} - \frac{1}{\overline{k}} \right) \left(\overline{(ka^2)} - \frac{\overline{(ka)}^2}{\overline{k}} \right) - \left(\overline{a} - \frac{\overline{(ka)}}{\overline{k}} \right)^2 \right\}^{1/2}.$$

Note that there is a typographical error in the equation [Eq. (14)] in Rosen and Hashin [35] as well as in the corresponding formula in the text by Christensen [7].

A bounded domain of possible effective bulk moduli and thermal strain coefficients for a specific choice of constituent phases is shown in Fig. 4. We found that the proposed design method did not yield pairs $(k^{(*)}, \alpha^{(*)})$ that were close to the Schapery-Rosen-Hashin bounds [Eq. (14)]. There were two possible explanations for this discrepancy: either the design method could not find the optimal solutions, or the bounds themselves could be improved upon. Indeed, the latter explanation turned out to be true.

Inspired by above mentioned discrepancy Gibiansky and Torquato [11] recently found improved bounds, which are also shown in Fig. 4. The new bounds can be written as

$$
\left. \begin{array}{c} \alpha^{(U)} \\ \alpha^{(L)} \end{array} \right\} = \frac{1}{k^{(*)}(k^{(U)} - k^{(L)})} \left\{ (k^{(U)} - k^{(*)})(k^{(L)} + \mu_{min}) \overline{\left(\frac{k\alpha}{k + \mu_{min}}\right)} + \right.
$$
$$
(k^{(*)} - k^{(L)})(k^{(U)} + \mu_{max}) \overline{\left(\frac{k\alpha}{k + \mu_{max}}\right)} \pm \tag{15}
$$
$$
\left. \Psi^{1/2} (k^{(U)} - k^{(*)})^{1/2} (k^{(*)} - k^{(L)})^{1/2} \right\},
$$

where

$$
\Psi = -(k^{(U)} + \mu_{max})(k^{(L)} + \mu_{min}) \left\{ \overline{\left(\frac{k\alpha}{k + \mu_{min}}\right)} - \overline{\left(\frac{k\alpha}{k + \mu_{max}}\right)} \right\}^2 +
$$
$$
(\mu_{max} - \mu_{min}) \left\{ (k^{(L)} + \mu_{min}) \overline{\left(\frac{k\alpha}{k + \mu_{min}}\right)}^2 - (k^{(U)} + \mu_{max}) \overline{\left(\frac{k\alpha}{k + \mu_{max}}\right)}^2 \right\} +
$$
$$
(k^{(U)} - k^{(L)}) \left\{ \overline{\left(\frac{k^2 \alpha^2}{k + \mu_{min}}\right)} + \mu_{max} \overline{\left(\frac{k\alpha^2}{k + \mu_{max}}\right)} - \overline{k\alpha^2} \right\},
$$

and $k^{(L)}$ and $k^{(U)}$ are the lower and upper Hashin-Shtrikman bounds on bulk modulus as given in Eq. (13). As will be seen in the subsequent section, the solutions obtained by the design procedure are very close to the new bounds.

Examination of the thermoelastic bounds in Fig. 4 reveals that extreme values (e.g. negative values) of thermal strain coefficients only are possible for low bulk moduli. If we simply tried to minimize/maximize the thermal strain $\alpha^{(*)}$, we would end up with a very weak material. Therefore, there is a tradeoff between extremizing thermal strain coefficients on the one hand and ending up with a stiff material on the other. This problem will be discussed in more detail in the next section.

15

4 Design examples

In this section, we will first discuss design examples with mixtures of hypothetical materials. These examples are used to benchmark the design algorithm for two- and three-phase design. We will also study other design examples that utilize real materials as constituent phases.

Plotting results

During the iterative procedure, a Postscript plot of the topology is generated every 10 iterations. The plot shows the current density and material distribution in the base cell, thus allowing the user to follow the evolution of the microstructure and interact if necessary. The plots in the following sections show the optimal density and material type distributions for the different design problems. If an element is dominating material phase two (i.e., $x_2^e > 0.5$), the element is illustrated by a cross with grey scale denoting the density x_1^e; white means void ($x_1^e = x_{min}$) and black means solid ($x_1^e = 1$). If the element is dominating material phase one (i.e., $x_2^e < 0.5$), it is shown as a filled rectangle with grey values interpreted as before. For all examples, we both show the resulting topologies represented by a single base cell (the design domain) and as a repeated microstructure consisting of 3 by 3 base cells.

4.1 Comparison with two-phase bounds

The two-phase bounds given by Eqs. (12) and (13) are used for benchmarking the design algorithm for two-phase design. The non-dimensionalized material data for the two phases are chosen as $E^{(2)}/E^{(1)} = 10$, $\nu^{(1)} = \nu^{(2)} = 0.3$, $\alpha^{(2)}/\alpha^{(1)} = 10$ and $c^{(1)} = c^{(2)} = 0.5$.

The bounds on the thermal strain coefficient for this mixture are found from Eq. (12) to be given by $6.3412 \leq \alpha^{(*)}/\alpha^{(1)} \leq 8.2524$ and the bounds on the bulk modulus are found from Eq. (13) to be given by $0.0996 \leq k^{(*)}/k^{(1)} \leq 0.1690$.

First we try to maximize the effective thermal strain coefficient which through Eq. (12) corresponds to maximizing the effective bulk modulus. Specifying macroscopic isotropy and horizontal and vertical geometric symmetry, the attained values with a 60 by 60 element discretization are $\alpha_{max}^{(*)}/\alpha^{(1)} = 8.2349$ and $k_{max}^{(*)}/k^{(1)} = 0.1680$. If we try to minimize the thermal strain coefficient we just get the "inverted" microstructure, meaning that the two domains are interchanged. The actual numbers obtained for this case are $\alpha_{min}^{(*)}/\alpha^{(1)} = 6.3907$ and $k_{min}^{(*)}/k^{(1)} = 0.1007$. The optimal topology of the microstructure for maximum thermal strain value and isotropy constraint is shown in Fig. 3 (top).

Relaxing the isotropy requirement by only specifying square symmetry (but still specifying horizontal and vertical geometric symmetry), the attained values with a 60 by 60 element discretization are $\alpha_{max}^{(*)} = 8.2320$ and $k_{max}^{(*)}/k^{(1)} = 0.1677$, $\alpha_{min}^{(*)} = 6.3733$ and $k_{min}^{(*)}/k^{(1)} = 0.1004$, respectively. The actual topology of the optimal two-phase microstructure is shown in Fig. 3 (bottom). As expected, the optimal microstructural topologies resemble the energy minimizing microstructures of Vigdergauz [45].

It should be noted that we get the same (except for numerical errors) effective properties for the isotropic material and square symmetric microstructures. This means, that the optimal rigidity Vigdergauz microstructures can be made isotropic by using the new geometry in Fig. 3 (top) instead of the one in Fig. 3 (bottom). Not surprisingly, it also shows that
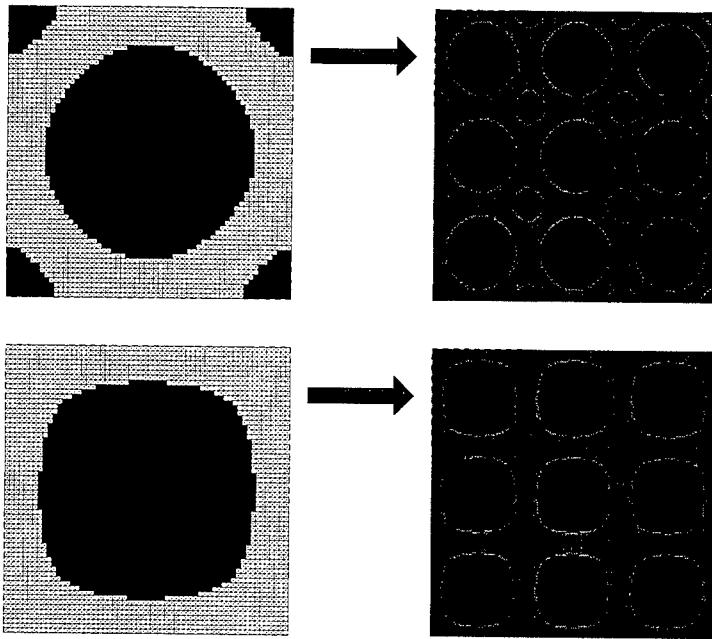
16

Figure 3: Optimal microstructures for two-phase design problem. Maximization of thermal strain coefficient with and without macroscopic isotropy constraint (top and bottom respectively). The filled regions consist of low expansion material (phase 1) and the cross-hatched regions consist of high expansion material (phase 2).

solutions with widely different topologies can have the same values of the objective function.

4.2 Comparison with three-phase bounds

The three-phase bounds given by Eqs. (13), (14) and (15) are used for benchmarking the design algorithm for three-phase design. The material data for the two phases are chosen as $E^{(1)}/E^{(2)} = 1$, $\nu^{(1)} = \nu^{(2)} = 0.3$, $\alpha^{(2)}/\alpha^{(1)} = 10$, and the volume fractions are prescribed to be $c^{(1)} = c^{(2)} = 0.25$ (i.e. $c^{(0)} = 0.5$). *Note that the volume fractions c_i are held fixed for this hypothetical composite, to allow for comparison with the bounds and for easy interpretation of the results.*
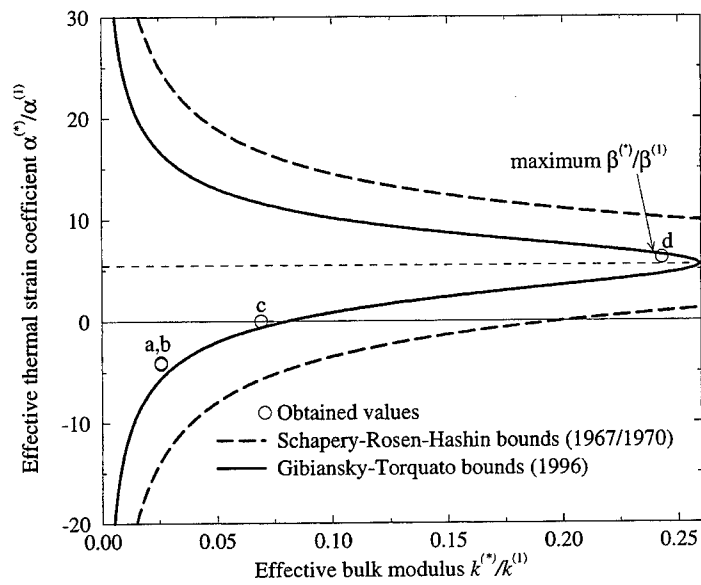
Figure 4: Bounds for three-phase design example. The circles with letters *a-d* denote the obtained values for the microstructures shown in Figs. 5 and 6.

Four three-phase design examples, constrained to be elastically isotropic, are considered as follows:

(a) Minimization of the *isotropic* thermal strain coefficient $\alpha^{(*)}/\alpha^{(1)}$ with a lower bound constraint on the effective bulk modulus given as 10% of the theoretically attainable bulk modulus, i.e. $k^{(*)}/k^{(1)} = 0.0258$. Horizontal geometric symmetry is specified.

(b) Same as design example (a) but with horizontal, vertical and diagonal (geometric) symmetry.

(c) Maximization of bulk modulus $k^{(*)}/k^{(1)}$ for fixed zero thermal expansion $\alpha^{(*)}/\alpha^{(1)} = 0$. Horizontal geometric symmetry is specified.

(d) Maximization of isotropic thermal stress coefficient $\beta^{(*)}/\beta^{(1)}$ with horizontal, vertical and diagonal geometric symmetry.

The old and new theoretical bounds are given by Eqs. (13) and (15), respectively, and they are shown Fig. 4. In examples (a) and (b), the lower bound on the possible thermal strain coefficient is $-5.567 \leq \alpha^{(*)}/\alpha^{(1)}$. In example (c), the upper bound on possible bulk modulus for zero thermal expansion is $k^{(*)}/k^{(1)} \leq 0.0692$. The upper bound on the thermal stress coefficient in design example (d) is $\beta^{(*)}/\beta^{(1)} \leq 3.15$ (for $k^{(*)}/k^{(1)} = 0.237$).

The resulting topologies are shown in Figs. 5 and 6 and their effective properties are shown in Table 1 and plotted as small circles in Fig. 4. Studying the graph in Fig. 4, we see that the obtained effective values are far away from the original Schapery-Rosen-Hashin bounds. This discrepancy inspired Gibiansky and Torquato to try to improve the bounds and indeed improvement was possible as seen in Fig. 4. The effective values of the examples (a)-(d) are still somewhat away from the improved bounds. This can be explained by the fact that the new bounds by Gibiansky and Torquato have not been proven to be optimal. Furthermore, it is our experience that a finer finite-element mesh makes it possible to get closer to the bounds. In example (a), the minimum thermal strain coefficient obtained for a 30 by 30 mesh is $\alpha^{(*)} = -3.59$ and $\alpha^{(*)} = -4.17$ for the 60 by 60 element discretization shown in Fig. 5. Due to computer time limitations, it has not been possible to try out finer discretizations.

The actual mechanisms behind the extreme thermal expansion coefficients of the materialstructures can be difficult to understand. To visualize one of the mechanisms, the (exaggerated) displacements, due to an increase in temperature of the microstructure in Fig. 5 (bottom), is shown in Fig. 7. Studying Fig. 7, we note that there appears to be contact between parts of the microstructure. This contact is only due to the magnification of the displacements used in the illustration. The simple linear modelling used here can not take such problems into account. Nevertheless, it would be interesting to extend the analysis to include non-linear behavior including contact, which would open up for a whole new world of interesting design possibilities. We will leave these extensions to future studies.

When allowing low bulk moduli [as in examples (a) and (b)], the main mechanism behind the extreme (negative) thermal expansion is the *reentrant cell structure* having bimaterial components which bend and cause large deformation when heated. The bimaterial interfaces of design examples (a) and (b) bend and make the cell contract, similar to the behavior
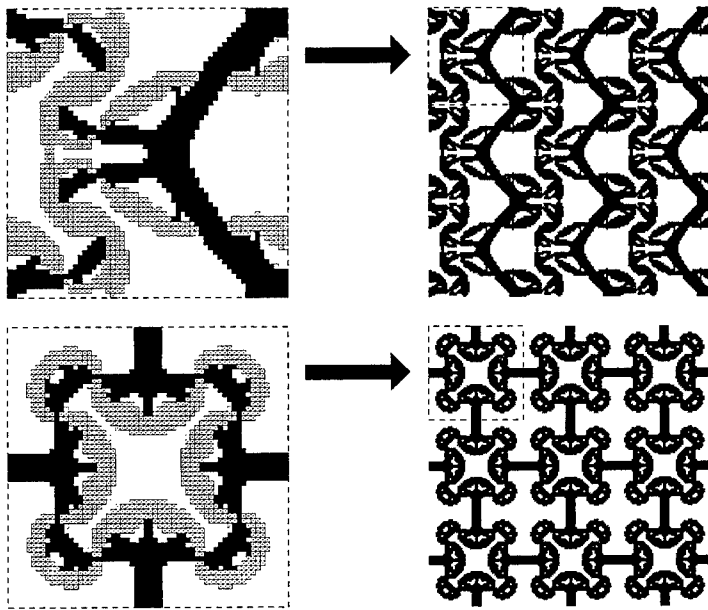
19

Figure 5: Examples (a) (top) and (b) (bottom): Optimal microstructures for minimization of effective thermal strain coefficient corresponding to the circles a and b in Fig. 4, respectively. The white regions denote void (phase 0), the filled regions consist of low expansion material (phase 1) and the cross-hatched regions consist of high expansion material (phase 2).
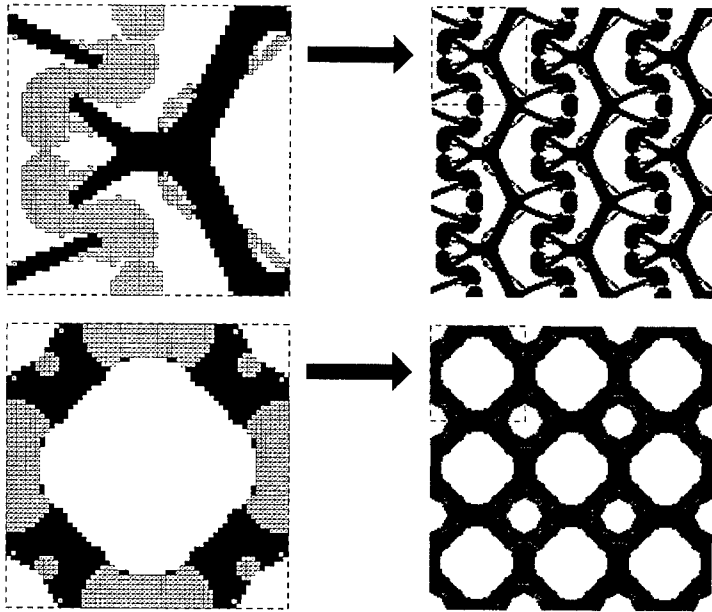
Figure 6: Examples **(c)** (top) and **(d)** (bottom): Optimal microstructures for maximization of bulk modulus with zero thermal expansion (top) and maximization of effective thermal stress coefficient (bottom) corresponding to the circles c and d in Fig. 4, respectively. The white regions denote void (phase 0), the filled regions consist of low expansion material (phase 1) and the cross-hatched regions consist of high expansion material (phase 2).
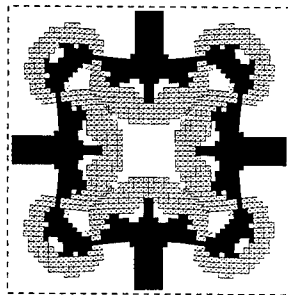
Figure 7: Thermal displacement of microstructure in Fig. 5 (bottom).

Example	Objective/ Constraint	$k^{(*)}/k^{(1)}$ (bound)	$\nu^{(*)}$	$\alpha^{(*)}/\alpha^{(1)}$ (bound)	$\beta^{(*)}/\beta^{(1)}$ (bound)
(a), Fig. 5	Min. $\alpha^{(*)}/\alpha^{(1)}$ $k^{(*)}/k^{(1)} \geq 0.0258$	0.0258	0.039	-4.17 (-5.567)	
(b), Fig. 5	Min. $\alpha^{(*)}/\alpha^{(1)}$ $k^{(*)}/k^{(1)} \geq 0.0258$	0.0258	0.51	-4.02 (-5.567)	
(c), Fig. 6	Max. $k^{(*)}/k^{(1)}$ $\alpha^{(*)}/\alpha^{(1)} \leq 0.0$	0.0692 (0.0814)	0.54	0	
(d), Fig. 6	Max. $\beta^{(*)}/\beta^{(1)}$	0.243	0.51		3.01 (3.15)

Table 1: Thermoelastic parameters for optimal three-phase microstructures composed of hypothetical materials compared with the bounds. The white regions denote void, the filled regions consist of low expansion material (phase 1) and the cross-hatched regions consist of high expansion material (phase 2).

of negative Poisson's ratio materials [24]. If a higher effective bulk modulus is specified, as in example (c), the intricate bi-material mechanisms are less pronounced resulting in a less extreme expansion ($\alpha_* = 0$). Finally, maximizing the expansive stress, as in example (d), results in a structure without bimaterial mechanisms, where the high expansion phase (cross hatched phase) is arranged such that it maximizes the horizontal and vertical expansion.

Design examples (a) and (b) in Fig. 5 demonstrate how two, topologically, very different microstructures can have (almost) the same value of the objective function. The only difference between the two examples is the specified geometric symmetry.

In order to check the validity of the effective values computed by the homogenization code, we will make a comparison between a simple example and an idealized beam model. Figure 8 shows the optimal microstructure (e) for maximization of the thermal strain coefficient in the vertical direction $\alpha_{22}^{(*)}$. We specify geometrical symmetry about horizontal and vertical axes, effective vertical stiffness component $C_{2222}^{(*)} \geq 0.07$ and volume fractions $c^{(1)}$ and $c^{(2)}$ less or equal 0.2. The obtained values are $\alpha_{11}^{(*)} = -20.7$ and $\alpha_{22}^{(*)} = 33.5$. The actual material volume fractions in the optimal topology are $c^{(1)} = 0.167$ and $c^{(2)} = 0.200$ and effective horizontal and vertical stiffness components are $k^{(*)} = 0.070$, respectively.

To check the obtained values, we calculate the effective thermal strain tensor using an idealized beam model in Appendix C. The predicted thermal strain coefficients and bulk modulus, are $\alpha_{11}^{(*)} = -21$, $\alpha_{22}^{(*)} = 32$ and $k^{(*)} = 0.085$, respectively. Good agreement between the idealized beam model and the effective properties is observed.
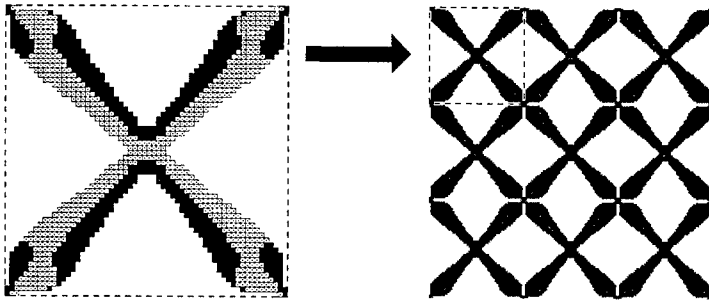
Figure 8: Example (e): Optimal microstructure for maximization of thermal strain in the vertical direction $\alpha_{22}^{(*)}$. The white regions denote void (phase 0), the filled regions consist of low expansion material (phase 1) and the cross-hatched regions consist of high expansion material (phase 2).

4.3 Mixtures of real materials

For the design of new materials with extreme thermal expansion coefficients, the two base materials should be of equal stiffness but widely differing thermal strain coefficients. Two materials fulfilling this requirement are isotropic Invar (Fe-36%Ni) and Nickel as discussed in the introduction. *For the next design examples, the volume fractions of the material phases are unconstrained.* This will allow for a wider range of minimum and maximum values, in contrast to the hypothetical examples (a)–(e) in which the volume fractions were fixed.

The material properties of Invar and Nickel can be found in the ASM-Handbook [1]. The Young's moduli are 150 GPa and 200 GPa, respectively, Poisson's ratios are 0.31 for both, and the thermal expansion coefficients are $0.8\mu m/(mK)$ and $13.4\mu m/(mK)$, respectively.

(f) Minimization of the *isotropic* thermal stress coefficient $\beta^{(*)}$. Horizontal geometric symmetry is specified.

(g) Minimization of the *vertical* thermal stress coefficient $\beta_{22}^{(*)}$. Horizontal and vertical symmetry is specified.

(h) Minimization of the *vertical* thermal stress $E_2^{(*)}\alpha_{22}^{(*)}$. Horizontal and vertical symmetry is specified.

(i) Maximization of the *vertical* strain $(\alpha_*)_{22}$ with constraint on vertical Young's modulus $E_2^{(*)} \geq 5$ GPa. Horizontal and vertical symmetry is specified.

The resulting topologies are shown in Figs. 9, 10 and 11, and their effective properties are shown in Table 2.

To overcome the positive thermal expansion of other surrounding materials, we seek to maximize the *contraction force*, i.e., minimize the isotropic thermal stress coefficient as in
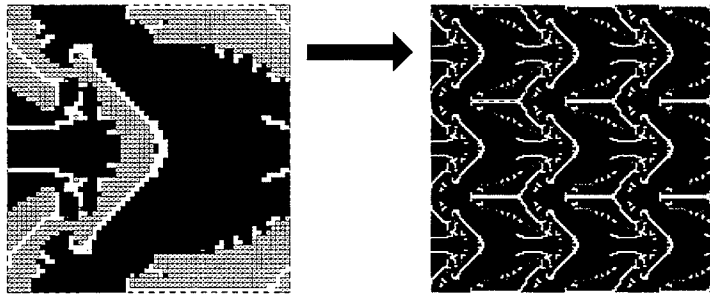
23

Figure 9: Examples (**f**): Optimal microstructure for minimization of the isotropic thermal stress coefficient $\beta^{(*)}$. The white regions denote void (phase 0), the filled regions consist of Invar (phase 1) and the cross-hatched regions consist of Nickel (phase 2).

Example	Objective	$\alpha^{(*)}$	$E^{(*)}$	$\nu^{(*)}$	$\beta^{(*)}$	$c^{(1)}/c^{(2)}$
		$\mu m/(mK)$	GPa		kPa/K	
Invar		0.8	150	0.31	175	1/0
Nickel	(Max. $\beta^{(*)}$)	13.4	200	0.31	3890	0/1
(**f**) Fig. 9	Min. $\beta^{(*)}$	-5.0	15	0.06	-78	0.60/0.28
(**g**) Fig. 10	Min. $\beta_{22}^{(*)}$	10.0/-1.6	9.2/8.8	-0.75/-0.80	258/-210	0.49/0.38
(**h**) Fig. 10	Min. $E_2^{(*)}\alpha_{22}^{(*)}$	5.4/-4.7	67/30	0.06/0.02	392/-128	0.60/0.30
(**i**) Fig. 11	Max. $\alpha_{22}^{(*)}$	23/35	1.1/5.0	-.14/-.62	2/174	0.38/0.46

Table 2: Thermoelastic parameters for optimal microstructures made of Invar (phase 1) and Nickel (phase 2).
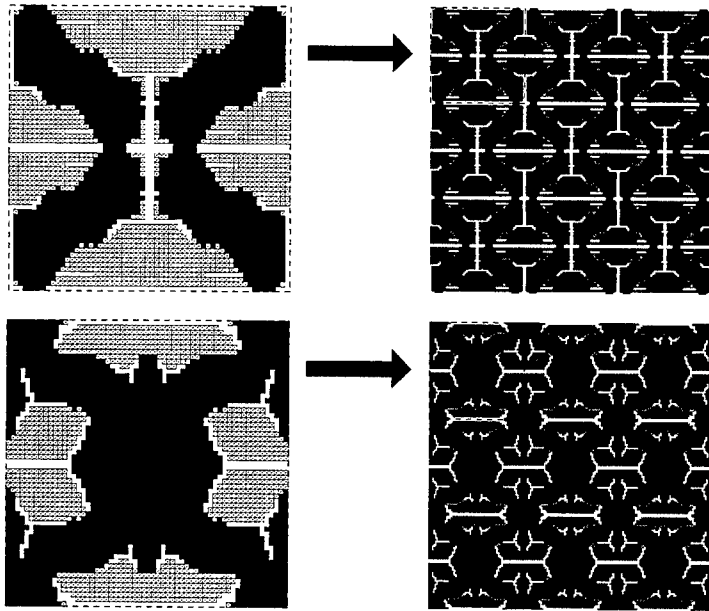
Figure 10: Examples **(g)** (top) and **(h)** (bottom): Optimal microstructures for minimization of thermal stress coefficient $\beta_{22}^{(*)}$ (top) and minimization of vertical contraction stress $E_2^{(*)}\alpha_{22}^{(*)}$. The white regions denote void (phase 0), the filled regions consist of Invar (phase 1) and the cross-hatched regions consist of Nickel (phase 2).
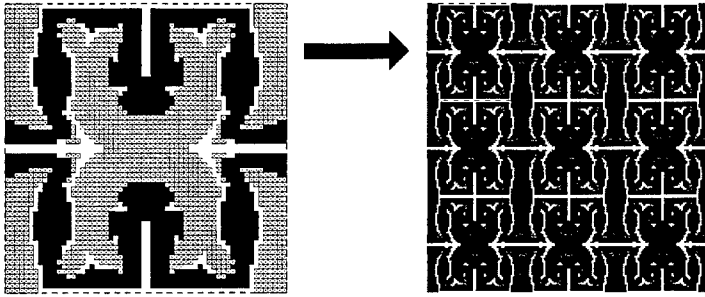
Figure 11: Example **(i)**: Optimal microstructure for maximization of thermal strain in the vertical direction $\alpha_{22}^{(*)}$. The white regions denote void (phase 0), the filled regions consist of Invar (phase 1) and the cross-hatched regions consist of Nickel (phase 2).

example **(f)**. The obtained *isotropic* contraction stress of example **(f)** is $\beta^{(*)} = -78\text{GPa}$. By relaxing the isotropy requirement and allowing orthotropic materials the *directional* contraction stress can be increased. In example **(g)** we minimize the value of $\beta_{22}^{(*)}$ and get the effective value $\beta_{22}^{(*)} = -128\text{GPa}$. Minimizing the value of $\beta_{22}^{(*)}$ gives us a composite which for *fixed boundaries* has high contraction force (remember that the thermal stress coefficient $\beta^{(*)}$ is the stress in a material constrained at the boundaries). If we want to maximize the contraction force for a material with free boundaries, we should minimize the product $(E_*)_2(\alpha_*)_{22}$ as done in example **(h)**. The "free boundary" stress of example **(g)** is $(E_*)_2(\alpha_*)_{22} = -14\text{GPa}$, whereas the "free boundary" stress of example **(g)** is $(E_*)_2(\alpha_*)_{22} = -141\text{GPa}$.

If we want to *maximize* the expansion stress of the composite, the best choice would be to take solid nickel material both for the isotropic and the directional cases.

The isotropic negative thermal expansion materials in examples **(a)**, **(b)** and **(f)** all have positive Poisson's ratios (0.04, 0.52 and 0.06, respectively), *showing that there is no mechanistic relationship between negative thermal expansion and negative Poisson's ratio*.

In example **(i)** we see again that allowing orthotropy can lead to high *directional* expansion coefficients. The vertical coefficient $(\alpha_*)_{22}$ of example **(i)** is 2.6 times higher than for solid nickel, but at the cost of a low vertical Young's modulus (2.5% of solid nickel).

26

5   Conclusions

We have proposed a method to design material microstructures with extreme thermoelastic properties. The optimization procedure has been shown to be very accurate in producing the optimal microstructures. Indeed, the results of this study motivated Gibiansky and Torquato to improve upon the 29-year old Schapery-Rosen-Hashin bounds on the thermal expansion of three-phase media. Our obtained values are close to the Gibiansky-Torquato bounds. We have shown that extreme thermal expansion behavior can be obtained but at the cost of a low bulk modulus. Therefore, there is a tradeoff between extremizing thermal strain coefficients on the one hand and ending up with a stiff material on the other. We have also shown that extreme directional thermal expansion can be obtained by allowing anisotropy of the composites.

For the topology optimization method in general, the results in this paper shows, that the method produces designs which are optimal indeed.

In practice, how can our optimally designed materials be manufactured? They may be fabricated (with cell sizes down to a few millimeters) using stereolithography techniques [20] or using surface micromachining techniques (with cell sizes down to 50 micros) as seen for materials with negative Poisson's ratios in Larsen, Sigmund and Bouwstra [26]. Furthermore, it will be interesting to examine whether the lessons learned from this continuum analyses can be exploited to optimally design and synthesis of materials at the molecular level (e.g. Baughman and Galvão [3]).

Finally, we note that the method is applicable to design of smart materials (piezoelectric or shape-memory-alloy inclusions). In a future paper, the procedure described here will be used to find the structures that optimize the piezoelectric properties of the material for use as actuators or sensors. The method can also be modified to handle three-dimensional microstructures. The extension to three dimensions is straight forward, but computer time will increase dramatically. Extensions to three dimensions for *two* material phases have been done in Sigmund [43] and Sigmund and Torquato [44].

References

[1] ASM. *ASM Handbook, volume 2: Properties and Selection*. The Materials Information Society, USA, 1993.

[2] M. Autio, M. Laitinen, and A. Pramila. Systematic creation of composites with prescribed thermomechanical properties. *Computational Engineering*, 3(3):249–259, 1993.

[3] R. Baughman and D. Galvão. Crystalline networks with unusual predicted mechanical and thermal properties. *Nature*, 365:735–737, 1993.

[4] M. Bendsøe and N. Kikuchi. Generating optimal topologies in optimal design using a homogenization method. *Computational Methods in Applied Mechanics and Engineering*, 71:197–224, 1988.

[5] A. Benssousan, J. L. Lions, and G. Papanicolau. *Asymptotic analysis for periodic structures*. North Holland, Amsterdam, 1978.

[6] J. Bourgat. Numerical experiments of the homogenization method for operators with periodic coefficients. In *Lecture notes in mathematics*, pages 330–356. Springer Verlag, Berlin, 1977.

[7] R. Christensen. *Mechanics of composite materials*. John Wiley and Sons, 1979.

[8] E. Collins and S. Richter. Linear-quadratic-gaussian-based controller design for Hubble space telescope. *journal of Guidance, Control, and Dynamics*, 18(2):208–213, 1995.

[9] A. Díaz and O. Sigmund. Checkerboard patterns in layout optimization. *Structural Optimization*, 10:40–45, 1995.

[10] G. Francfort and F. Murat. Homogenization and optimal bounds in linear elasticity. *Archieves of Rational Mechanical Analysis*, 94:307–334, 1986.

[11] L. Gibiansky and S. Torquato. Thermal expansion of isotropic multi-phase composites and polycrystals. *In preparation*, 1996.

[12] Y. Grabovsky and R. Kohn. Microstructures minimizing the energy of a two phase elastic composite in two space dimensions. I: the confocal ellipse construction. *journal of the Mechanics and Physics of Solids*, 43(6):933–947, 1995.

[13] Y. Grabovsky and R. Kohn. Microstructures minimizing the energy of a two phase elastic composite in two space dimensions. II: the Vigdergauz microstructure. *journal of the Mechanics and Physics of Solids*, 43(6):949–972, 1995.

[14] J. Guedes and N. Kikuchi. Preprocessing and postprocessing for materials based on the homogenization method with adaptive finite element methods. *Computer methods in applied mechanical engineering*, 83:143–198, 1991.

[15] R. Haber, C. Jog, and M. Bendsøe. A new approach to variable-topology shape optimization using a constraint on perimeter. *Structural Optimization*, 11:1–12, 1996.

28

[16] R. Hanson and K. Hiebert. A sparse linear programming subprogram. Technical Report Report SAND81-0297, Sandia National Laboratories, 1981.

[17] Z. Hashin and S. Shtrikman. A variational approach to the theory of the elastic behaviour of multiphase materials. *Journal of the Mechanics and Physics of Solids*, pages 127–140, March–April 1963.

[18] G. Hausch, R. Bächer, and J. Hartmann. Influence of thermomechanical treatment on the expansion behavior of invar and superinvar. *Physica B*, 161:22–24, 1989.

[19] S. Hollister and B. Riemer. Digital image based finite element analysis for bone microstructure using conjugate gradient and Gaussian filter techniques. In *SPIE, volume 2035 Mathematical Methods in Medical Imaging II*, pages 95–106, 1993.

[20] P. Jacobs. *Rapid prototyping and manufacturing – Fundamentals of Stereolithography*. SME, Dearborn, MI, USA, 1992.

[21] C. Jog and R. Haber. Stability of finite elements for distributed-parameter optimization and topology design. *Tam-report No. 758*, 1994. University of Illinois at Urbana-Champaign.

[22] H.-M. Kagaya and T. Soma. Compression effect on specific heat and thermal expansion of Si and Ge. *Solid State Communications*, 85(7):617–621, 1993.

[23] R. Kohn and G. Strang. Optimal design and relaxation of variational problems. *Communications Pure in Applied Mathematics and Mechanics*, 39:1–25, 139–182, 353–377, 1986. (Three parts).

[24] R. Lakes. Foam structures with negative Poisson's ratio. *Science*, 235:1038, 1987.

[25] R. Lakes. Materials with structural hierarchy, review article. *Nature*, 361:511–515, 1993.

[26] U. Larsen, O. Sigmund, and S. Bouwstra. Design and fabrication of compliant mechanisms and material structures with negative Poisson's ratio. In *IEEE, International Workshop on Micro Electro Mechanical Systems, MEMS-96*, 1996.

[27] V. Levin. Thermal expansion coefficients of heterogeneous materials. *Mekhanika Tverdoga Tela*, 2:88–94, 1967.

[28] G. Milton and A. Cherkaev. Which elasticity tensors are realizable? *Journal of engineering materials and technology, Transactions of the ASME*, 117(4):483–493, 1995.

[29] H. Mlejnik and R. Schirrmacher. An engineering approach to optimal material distribution and shape finding. *Computational Methods in Applied Mechanics and Engineering*, 106:1–26, 1993.

[30] M. Mullender, R. Huiskes, and H. Weihnans. A physiological approach to the simulation of bone remodelling as a self-organizational controll process. *journal of Biomechanics*, 11:1389–1394, 1994.

[31] V. Parton and B. Kudryavtsev. *Engineering Mechanics of Composite Structures.* CRC Press, 1993.

[32] P. Pedersen. On the minimum mass layout of trusses. In *AGARD conference proceedings No. 36, Symposium on structural optimization*, pages 189–192, 1970.

[33] W. Press, S. Teukolsky, W. Vetterling, and B. Flannery. *Numerical recipes in Fortran.* Cambridge University Press, 1992.

[34] H. Rodriques and P. Fernandes. A material bases model for topology optimization of thermoelastic structures. *International journal for numerical methods in engineering,* 38:1951–1965, 1995.

[35] B. Rosen and Z. Hashin. Effective thermal expansion and specific heat of composite materials. *International journal of Engineering Science,* 8:157–173, 1970.

[36] G. Rozvany, M. Zhou, T. Birker, and O. Sigmund. Topology optimization using iterative continuum type optimality criteria (COC) methods for discretized systems. In M. Bendsøe and C. Soares, editors, *Topology Design of Structures,* pages 273–286. Springer, 1992.

[37] E. Sanchez-Palencia. Non-homogeneous media and vibration theory. In *Lecture notes in physics.* Springer Verlag, Berlin, 1980.

[38] R. Schapery. Thermal expansion coefficients of composite materials based on energy principles. *Journal of composite materials,* 2(3):380–404, 1968.

[39] K. Schittkowski. Numerical comparison of non-linear programming algorithms for structural optimization. *Structural Optimization,* 7(1–2):1–19, 1994.

[40] P. Schultz and H. Smyth. *Amorphous Materials,* chapter 44, Ulta-low-expansion glasses and their structure in the $SIO_2 - TiO_2$ system, pages 453–462. Wiley, New York, 1970.

[41] O. Sigmund. *Design of material structures using topology optimization.* PhD thesis, Department of Solid Mechanics, Technical University of Denmark, December 1994.

[42] O. Sigmund. Materials with prescribed constitutive parameters: an inverse homogenization problem. *International journal of Solids and Structures,* 31(17):2313–2329, 1994.

[43] O. Sigmund. Tailoring materials with prescribed elastic properties. *Mechanics of Materials,* 20:351–368, 1995.

[44] O. Sigmund and S. Torquato. On the design of 1-3 piezocomposites using topology optimization. *In preparation,* 1996.

[45] S. Vigdergauz. Regular structures with extremal elastic properties. *Mechanics of Solids,* 24(3):57–63, 1989.

[46] S. Vigdergauz. Three-dimensional grained composites of extreme thermal properties. *journal of the Mechanics and Physics of Solids*, 42(5):729–740, 1994.

[47] R. Wetherhold and J. Wang. Tailoring thermal deformation by using layered beams. *Composites Science and Technology*, 53:1–6, 1995.

[48] Z. Yang, M. Yewondwossen, D. Lawther, S. Ritcey, D. Geldart, and R. Dunlap. Thermal expansion of $Bi_{2.2}Sr_{1.8}CaCu_2O_x$ superconducter single crystals. *journal of Superconductivity*, 8(2):233–239, 1995.

A Homogenization theory

This appendix summarizes the important equations for computation of the effective thermoelastic properties of a periodic inhomogeneous material using the homogenization theory as developed in Bensoussan et al. [5] and Sanchez-Palencia [37].

We want to find the effective homogenized thermoelastic tensors $C_{ijkl}^{(*)}$, $\beta_{ij}^{(*)}$ and $\alpha_{ij}^{(*)}$ of a periodic material microstructure described by the rectangular base cell Y. Using the symmetries of the thermoelastic tensors, $C_{ijkl} = C_{jikl} = C_{ijlk} = C_{klij}$, $\beta_{ij} = \beta_{ji}$ and $\alpha_{ij} = \alpha_{ji}$, the anisotropic elasticity tensor has nine and the thermal expansion tensors have three independent parameters.

Only considering first order terms in the asymptotic expansion, it can be shown that relations for obtaining the effective elasticity, thermal stress and thermal strain tensors can be written in energy forms as

$$
\begin{aligned}
C_{pqrs}^{(*)}\epsilon_{pq}^{0(kl)}\epsilon_{rs}^{0(ij)} &= \frac{1}{Y}\int_Y C_{pqrs}(\epsilon_{pq}^{0(kl)} - \epsilon_{pq}^{(*)}(\chi^{kl}))(\epsilon_{rs}^{0(ij)} - \epsilon_{rs}^{(*)}(\chi^{ij}))dY, \\
\beta_{kl}^{(*)}\epsilon_{kl}^{0(ij)} &= \frac{1}{Y}\int_Y C_{pqkl}(\alpha_{pq} - \epsilon_{pq}^C(\Gamma))(\epsilon_{kl}^{0(ij)} - \epsilon_{kl}^{(*)}(\chi^{ij}))dY, \\
\alpha_{ij}^{(*)} &= (C_{ijkl}^{(*)})^{-1}\beta_{kl}^{(*)},
\end{aligned}
\tag{16}
$$

where the displacements fields χ^{kl} and Γ are solutions to the following cell problems: find $\chi^{kl} \in V$ and $\Gamma \in V$, such that

$$
\begin{aligned}
\int_Y C_{ijpq}\frac{\partial \chi_p^{kl}}{\partial y_q}\frac{\partial v_i}{\partial y_j}dY &= \int_Y C_{ijpq}\frac{\partial v_i}{\partial y_j}dY, \qquad \forall v \in V, \\
V &= \{v \;:\; v\ is\ Y-periodic\}, \\[2mm]
\int_Y C_{ijkl}\frac{\partial \Gamma_k}{\partial y_l}\frac{\partial v_i}{\partial y_j}dY &= \int_Y \beta_{ij}\frac{\partial v_i}{\partial y_j}dY, \qquad \forall v \in V, \\
V &= \{v \;:\; v\ is\ Y-periodic\}.
\end{aligned}
\tag{17}
$$

The fluctuation strains $\epsilon_{pq}^{*(kl)}(\chi^{kl})$ and $\epsilon_{pq}^C(\Gamma)$ are defined through the strain-displacement relations $\epsilon_{pq}^{(*)}(\chi^{kl}) = \frac{1}{2}(\partial \chi_p^{kl}/\partial y_q + \partial \chi_q^{kl}/\partial y_p)$ and $\epsilon_{pq}^C(\Gamma) = \frac{1}{2}(\partial \Gamma_p/\partial y_q + \partial \Gamma_q/\partial y_p)$ and $\epsilon_{pq}^{0(kl)}$ are three linearly independent test strain fields. In Eqs. (16) and (17), C_{ijkl}, β_{ij} and α_{ij}

are the locally (dependent on **y**) varying stiffness, thermal stress and thermal strain tensors, respectively.

As test strain fields $\epsilon_{pq}^{0(kl)}$ we choose the three unit tensors (in two dimensions) $\epsilon_{pq}^{0(11)} = (1,0,0,0)$, $\epsilon_{pq}^{0(22)} = (0,1,0,0)$ and $\epsilon_{pq}^{0(12)} = (0,0,1,0)$ and $\epsilon_{pq}^{0(21)}$ can be ignored for symmetry reasons.

The equilibrium equations, Eqs. (17), are solved using the finite-element method. The base cell is discretized by finite elements and solving Eqs. (17) means solving a finite-element problem with periodic boundary conditions for the three different prestrain cases: horizontal unit strain, vertical unit strain, shear unit strain as given by the tensors $\epsilon_{pq}^{0(kl)}$ and for a thermal strain field resulting from the locally varying thermal stress tensor β_{ij}.

Having discretized the base cell by N finite elements, the integrals for the evaluation of the homogenized properties in Eqs. (16) can be evaluated on the element level and the effective properties can be written as the sums

$$
C_{ijkl}^{(*)} = \frac{1}{Y} \sum_{e=1}^{N} \int_{Y^e} C_{pqrs}^e (\epsilon_{pq}^{0(kl)} - \epsilon_{pq}^{(*)}(\chi^{kl}))(\epsilon_{rs}^{0(ij)} - \epsilon_{rs}^{(*)}(\chi^{ij})) dY^e,
$$

$$
\beta_{ij}^{(*)} = \frac{1}{Y} \sum_{e=1}^{N} \int_{Y^e} C_{pqkl}^e (\alpha_{pq} - \epsilon_{pq}^C(\Gamma))(\epsilon_{kl}^{0(ij)} - \epsilon_{kl}^{(*)}(\chi^{ij})) dY^e.
$$

(18)

where Y^e is the area of element e.

For a more thorough description of the numerical homogenization procedure and finite-element discretization, the reader is referred to the numerical works of Bourgat [6] and Guedes and Kikuchi [14].

To solve the linear system of equations we use a so-called Element-By-Element Preconditioned-Conjugate-Gradient solver (EBE-PCG). The PCG solver is described in Numerical Recipes [33] and its application to finite element problems is discussed in Hollister and Riemer [19], who use the method for the microstructural analysis of human bone structure discretized by up to one million finite elements. The advantages gained by using the EBE-PCG solver for the present design method are multiple. The EBE-PCG solver is an iterative solver using a starting guess for the displacement vector. By using the displacement vector from the preceding design step, computational time can be saved. Furthermore, we do not need an exact solution to the finite-element problem in the beginning of the design sequence, thus we can stop the solver when an approximate solution has been reached. Only in the final iterations of the optimization procedure we need an exact solution and then, the convergence requirements of the solver can be made stricter. Another advantage of the EBE-PCG solver is, that is does not require an assembly of the global stiffness matrix thereby saving storage space, in fact, it is only necessary to store two element stiffness matrices, implying that the stiffness matrix for a particular element can be calculated using Eq. (4). Finally, the EBE-PCG solver eliminates problems with increase of bandwidth due to the periodic boundary conditions. Opposing nodes of the base cells are simply given the same node numbers causing no increase in computational complexity, due to the element-by-element nature of the EBE-PCG solver.

32

B Sensitivity analysis

This appendix derives all the sensitivities which are necessary to solve the sequential linear programming problem Eq. (10). The sensitivities can be found directly from the strain fields already computed by the homogenization procedure.

The sensitivities of the effective stiffness tensor in Eq. (18) with respect to design variables x_1^e and x_2^e of element e can be found as

$$\frac{\partial C_{ijkl}^{(*)}}{\partial x_m^e} = -\frac{1}{Y}\int_{Y^e}\frac{\partial C_{pqrs}^e}{\partial x_m^e}(\epsilon_{pq}^{0(kl)} - \epsilon_{pq}^{(*)}(\chi^{kl}))(\epsilon_{rs}^{0(ij)} - \epsilon_{rs}^{(*)}(\chi^{ij}))dY^e, \ m = 1,2, \qquad (19)$$

where it was used that the test fields $\epsilon_{ij}^{0(kl)}$ are independent of the design variables (i.e. $\partial\epsilon_{ij}^{0(kl)}/\partial x_1^e = \partial\epsilon_{ij}^{0(kl)}/\partial x_2^e = 0$).

The sensitivities of the local stiffness tensor are

$$\frac{\partial C_{ijkl}^e}{\partial x_1^e} = (1 - x_2^e)C_{ijkl}^{(1)} + x_2^e C_{ijkl}^{(2)} \quad \text{and} \quad \frac{\partial C_{ijkl}^e}{\partial x_2^e} = x_1^e(-C_{ijkl}^{(1)} + C_{ijkl}^{(2)}). \qquad (20)$$

Sensitivity of the effective thermal stress tensor with respect to design variable x_1^e in Eq. (18) can be found as

$$\frac{\partial\beta_{ij}^{(*)}}{\partial x_1^e} = -\frac{1}{Y}\int_{Y^e}\frac{\partial C_{pqkl}^e}{\partial x_1^e}(\alpha_{pq} - \epsilon_{pq}^C(\Gamma))(\epsilon_{kl}^{0(ij)} - \epsilon_{kl}^{(*)}(\chi^{ij}))dY^e, \qquad (21)$$

where it was used that the thermal test field α_{ij} is independent of design variable x_1^e (i.e. $\partial\alpha_{ij}/\partial x_1^e = 0$).

As α_{ij} is dependent on design variable x_2^e (i.e. $\partial\alpha_{ij}^e/\partial x_2^e = -\alpha_{ij}^{(1)} + \alpha_{ij}^{(2)}$), sensitivity of the effective thermal tensor with respect to design variable x_2^e in Eq. (18) has an extra term

$$\frac{\partial\beta_{ij}^{(*)}}{\partial x_2^e} = -\frac{1}{Y}\int_{Y^e}\frac{\partial C_{pqkl}^e}{\partial x_2^e}(\alpha_{pq} - \epsilon_{pq}^C(\Gamma))(\epsilon_{kl}^{0(ij)} - \epsilon_{kl}^{(*)}(\chi^{ij}))dY^e +$$
$$\frac{1}{Y}\int_{Y^e}C_{pqkl}^e\frac{\partial\alpha_{pq}^e}{\partial x_2^e}(\epsilon_{kl}^{0(ij)} - \epsilon_{kl}^{(*)}(\chi^{ij}))dY^e. \qquad (22)$$

Sensitivities of the effective thermal strain tensor $\alpha_{ij}^{(*)}$ with respect to design variables x_1^e and x_2^e are found by differentiating Eq. (16) as follows:

$$\frac{\partial\alpha_{ij}^{(*)}}{\partial x_m^e} = \frac{\partial(C_{ijkl}^{(*)})^{-1}}{\partial x_m^e}\beta_{kl}^{(*)} + (C_{ijkl}^{(*)})^{-1}\frac{\partial\beta_{kl}^{(*)}}{\partial x_m^e}, \ m = 1,2. \qquad (23)$$

Finally, the sensitivities of the volume fractions Eqs. (5) with respect to design variables x_1^e and x_2^e are

$$\begin{aligned}
\partial c^{(1)}/\partial x_1^e &= (1 - x_2^e)Y^e/Y, & \partial c^{(1)}/\partial x_2^e &= x_1^e Y^e/Y, \\
\partial c^{(2)}/\partial x_1^e &= x_2^e Y^e/Y, & \partial c^{(2)}/\partial x_2^e &= x_1^e Y^e/Y.
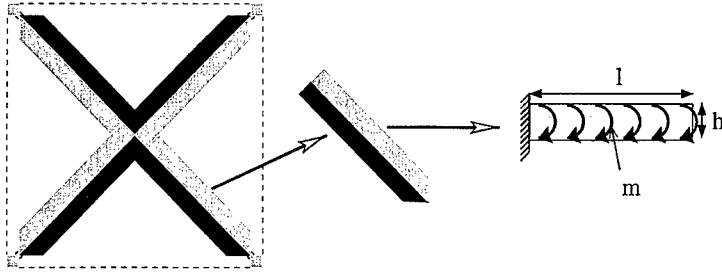\end{aligned} \qquad (24)$$

33

Figure 12: Idealization of the cross microstructure from Fig. 8.

C Beam model of thermal actuator example

To check the results obtained with the topology optimization algorithm, this appendix calculates the effective thermal strain tensor for the "maximization of vertical expansion" (Fig. 8) example (e) using a simple beam model.

The cross-like topology from Fig. 8 can be idealized as seen in Fig. 12. In the interpretation we assume that each of the four legs are slender beams of height h, width $w = 1$ and length $l = \sqrt{2}/2$. The four beam legs are joined together at the center of the cell and connected to neighboring cells with ideal moment-free hinges.

The thermal strain coefficient of the beam model can be found by calculating the bending and elongation of each "leg" and projecting these displacements to the horizontal and vertical directions. Using Bernoulli-Euler beam theory, the strain across the thickness of a beam varies with the distance from the neutral axis as $\epsilon_x = y/r$, where ϵ_x is the strain in the x-direction (horizontal) and r is the radius of curvature. Using Hooke's law, the stress in the x-direction of the beam is $\sigma_x = E\epsilon_x = Ey/r$. The thermal expansion of the two layers can be seen as an applied thermal stress to the two layers, i.e., $\sigma_{T(i)} = E\alpha_i$ ($i = 1, 2$). To find the beam moment-curvature relationship, resulting moments about the transverse beam-axis are summed to give

$$w \int_{-h/2}^{h/2} \sigma_T y \, dy = w \int_{-h/2}^{h/2} \sigma_x y \, dy \tag{25}$$

or

$$w \int_{-h/2}^{0} E\alpha^{(1)} y \, dy - w \int_{0}^{h/2} E\alpha^{(2)} y \, dy = w \int_{-h/2}^{h/2} E\frac{y^2}{r} \, dy. \tag{26}$$

Eq. (26) can be evaluated as

$$w\frac{1}{8} Eh^2 \alpha^{(1)} y - w\frac{1}{8} Eh^2 \alpha^{(2)} y = wE\frac{h^3}{12r}. \tag{27}$$

Using the approximation $d^2y/dx^2 \approx 1/r$, the differential equation for bending of the beam can be found as

$$\frac{d^2y}{dx^2} = \frac{1}{r} = \frac{3(\alpha^{(1)} - \alpha^{(2)})}{2h}. \tag{28}$$

34

Integrating Eq. (28) twice with respect to x, we get the vertical displacement at the tip of the cantilever

$$u_y = \frac{3l^2(\alpha^{(1)} - \alpha^{(2)})}{4h}.$$ (29)

The displacement in the x-direction is simply the average elongation

$$u_x = l(\alpha^{(1)} + \alpha^{(2)})/2.$$ (30)

Rotating the leg 45 degrees, the resulting deflection of one leg in the horizontal and vertical directions are

$$u_h = \frac{\sqrt{2}}{2}(u_x + u_y) \quad \text{and} \quad u_v = \frac{\sqrt{2}}{2}(-u_x + u_y).$$ (31)

The effective thermal strain coefficients are the relative displacements of the whole cross in the horizontal and vertical directions, respectively

$$\alpha_{11}^{(*)} = \frac{2u_h}{l_x} = \frac{\sqrt{2}(u_x + u_y)}{l_x} = \frac{\sqrt{2}}{l_x}\left(l(\alpha^{(1)} + \alpha^{(2)})/2 + \frac{3l^2(\alpha^{(1)} - \alpha^{(2)})}{4h}\right),$$

$$\alpha_{22}^{(*)} = -\frac{2u_v}{l_y} = -\frac{\sqrt{2}(-u_x + u_y)}{l_y} = \frac{\sqrt{2}}{l_y}\left(l(\alpha^{(1)} + \alpha^{(2)})/2 - \frac{3l^2(\alpha^{(1)} - \alpha^{(2)})}{4h}\right).$$ (32)

Finally, by inserting $l = \sqrt{2}/2$, we get

$$\alpha_{11}^{(*)} = \frac{1}{2l_x}(\alpha^{(1)} + \alpha^{(2)}) \pm \frac{3\sqrt{2}}{8hl_x}(\alpha^{(1)} - \alpha^{(2)}).$$ (33)

The thickness of the legs in Fig. 8 is estimated to $h = 0.18$. Inserting this value together with material data in Eq. (33), we get $\alpha_{11}^{(*)} = -21$ and $\alpha_{22}^{(*)} = 32$.

Again using simple beam analysis, the effective bulk modulus can be found as $k^{(*)} \approx 16Ewh^3$. Inserting $h = 0.18$ and $w = 1$, we get $k^{(*)} \approx 0.085$.